

# Infrared characterization of amorphous and polycrystalline D<sub>2</sub>O ice on controlled wettability self-assembled alkanethiolate monolayers

Isak Engquist, Ingemar Lundström, and Bo Liedberg<sup>a)</sup>  
*Molecular Films and Surface Analysis Group, Laboratory of Applied Physics, Linköping University,  
S-581 83, Linköping, Sweden*

Atul N. Parikh<sup>b)</sup> and David L. Allara  
*Department of Materials Science and Engineering and Department of Chemistry,  
The Pennsylvania State University, University Park, Pennsylvania 16802*

(Received 11 July 1996; accepted 22 November 1996)

Infrared reflection–absorption spectroscopy has been used to characterize thin overlayers (1–200 Å) of D<sub>2</sub>O ice deposited in UHV onto a set of self-assembled alkanethiolate monolayers (SAMs) of controlled wettabilities on gold. The SAMs were prepared from a series of controlled composition, mixed solutions of HS(CH<sub>2</sub>)<sub>15</sub>CH<sub>3</sub> and HS(CH<sub>2</sub>)<sub>16</sub>OH, making it possible to investigate the whole wettability range from  $\theta \approx 0^\circ$  to  $\theta = 112^\circ$ , where  $\theta$  is the static contact angle with water. Dosing of D<sub>2</sub>O and infrared measurements were carried out at selected sample temperatures between 82 and 150 K. Experimental spectra of ice overlayers recorded below 100 K on all SAM substrates are in good agreement with simulated reflection–absorption spectra, derived from the optical constants of amorphous ice. This agreement allows accurate film thickness determination. In contrast, lack of correspondence in spectral signature is noted between the spectra of annealed films and simulated polycrystalline (or amorphous) ice spectra. We interpret this discrepancy to suggest that significant substrate-induced differences between thin overlayers and bulk ice persist in the latter case. Spectral indications of ice–substrate interaction are also seen for amorphous ice, and are especially prominent in the case of highly hydrophobic (pure CH<sub>3</sub>-terminated,  $\theta = 112^\circ$ ) substrates. In this case the substrate effect extends up to an *average* film thickness (150–200 Å) corresponding to  $\sim 50$  ice monolayers, in contrast to highly hydrophilic OH-terminated substrates where the substrate effects appear to vanish beyond  $\sim 5$  monolayers (15–20 Å average thickness). Annealing of thin ice overlayers (2–3 monolayers) clearly demonstrates a strong correlation between the onset as well as progression of the transition from amorphous to polycrystalline ice and the exact substrate wettability or chemical composition. The data further suggest the existence of metastable intermediate forms, that are neither purely amorphous nor polycrystalline. We discuss these observations in terms of substrate–overlayer interaction. A tentative “phase diagram” summarizing these results is presented. © 1997 American Institute of Physics. [S0021-9606(97)51408-5]

## INTRODUCTION

Since the first report in 1983,<sup>1</sup> self-assembled alkanethiolate monolayers (SAMs) on gold have received continuously increasing attention as model organic surfaces of controlled chemical structure and composition.<sup>2</sup> During the most recent years, an increasing number of studies have been dealing with the potential applications of SAMs, in such diverse areas as molecular recognition,<sup>3,4</sup> surface biology and biochemistry,<sup>5–7</sup> chemical force microscopy,<sup>8,9</sup> metallization of organic materials,<sup>10</sup> corrosion protection,<sup>11</sup> molecular crystal growth,<sup>12</sup> alignment of liquid crystals,<sup>13</sup> pH-sensing devices,<sup>14</sup> patterned surfaces on the  $\mu\text{m}$  scale,<sup>15,16</sup> and lithographic resists.<sup>17</sup> In several of these areas, a fundamental understanding of the interaction between SAMs and secondary adsorbates is crucial. For example, in biochemical applications where water–organic interfaces are ubiquitous and in

studies of the molecular basis of wetting and of hydrogen bonding interactions, the importance of water as the secondary adsorbate cannot be overestimated.<sup>18–20</sup> For these reasons, we are performing a series of model experiments to systematically evaluate the interactions of water with a large set of SAMs of single and mixed chemical functionalities.<sup>21,22</sup> As a matter of further interest, the formation, ordering, and phase behavior of interface-confined solid water films, i.e., ice, constitute a research topic in its own right,<sup>23–25</sup> with possible applications in astrophysical research, biochemistry, and in the fundamental understanding of liquid water.

In a previous study,<sup>21</sup> we have investigated D<sub>2</sub>O adsorption on mixed CH<sub>3</sub>-/OH-terminated SAM substrates using temperature programmed desorption (TPD) and, to a limited extent, infrared reflection–absorption spectroscopy (IRAS). We concluded that a structural transition from amorphous to polycrystalline ice occurs, with an onset temperature that varies from  $\sim 110$  K on pure CH<sub>3</sub>-terminated substrates to  $\sim 150$  K on pure OH-terminated substrates. Further, the TPD experiments revealed an almost constant D<sub>2</sub>O desorp-

<sup>a)</sup> Author to whom correspondence should be addressed. Electronic mail: bol@ifm.liu.se

<sup>b)</sup> Current address: Los Alamos National Laboratory, Chemical Science and Technology Division, MS G755, Los Alamos, New Mexico 87545.

tion peak temperature for SAMs with water contact angles from about 112° (pure CH<sub>3</sub>;  $\cos \theta = -0.4$ ) down to ~50° ( $\cos \theta = 0.6$ ). Around  $\theta = 50^\circ$ , an abrupt increase in the desorption peak temperature by about 4 K occurs, followed by constant peak temperature in the  $\theta = 40^\circ$  ( $\cos \theta = 0.8$ ) to  $\theta = 8^\circ$  (pure OH;  $\cos \theta = 1.0$ ) region. We interpret this sudden change to represent a limiting case where the adsorbate, due to hydrogen bonding to the SAM substrate, is no longer fully converted to polycrystalline ice from its initial amorphous state before desorption occurs.

This paper is a continuation of the previous work, where we will demonstrate the use of IRAS to characterize the nature of ice overlayers on SAM substrates, addressing both overlayer structure and thickness, and how the composition and wettability of the SAM substrate influence the ice overlayer at different temperatures. To this end, we will compare the measured spectra with semiempirical model simulations of spectra based on the optical constants of amorphous and polycrystalline ice and describe how the comparison may be used to draw conclusions about overlayer structure and thickness. Thin ice films, a few monolayers in thickness, are the main objective of this investigation, although some similarities and differences in relation to bulk ice will be highlighted.

## EXPERIMENT

A detailed account of preparation and measurement procedures has been given elsewhere<sup>21</sup> and only a brief description is given here. Gold films were prepared by electron beam evaporation of 10 Å of Cr or Ti followed by 2000 Å of Au onto clean silicon wafers. Highly hydrophobic ( $\theta \geq 112^\circ$ ) and completely hydrophilic ( $\theta \sim 10^\circ$ ) substrates were made by immersing these wafers in 2 mM ethanolic (99.5%) solutions of HS(CH<sub>2</sub>)<sub>15</sub>CH<sub>3</sub> (TCH<sub>3</sub>) and HS(CH<sub>2</sub>)<sub>16</sub>OH (TOH), respectively. Mixed 2 mM solutions of these thiols in controlled, variable proportions were used to obtain intermediate wettability substrates.

Static contact angles were measured by imaging a drop of deionized (>18 MΩ cm) water with a video camera equipped with a microscope lens. Each reported angle is the average of six measurements on the same surface.

Ellipsometric characterization was performed using an automatic null ellipsometer (Rudolph Research AutoEl III). The measurement output ( $\Delta$  and  $\Psi$ ) was used to calculate the thiol monolayer thickness, following the algorithm by McCrackin<sup>26</sup> and assuming a three-layer parallel slab Au/thiol/air model and an isotropic refractive index of  $n = 1.50$ ,  $k = 0$  of the thiol monolayer.<sup>27</sup>

For infrared precharacterization of the SAMs a Bruker IFS113v FTIR spectrometer with a grazing angle accessory<sup>28</sup> aligned at 83° incidence angle was employed. *p*-polarized light and *f*/4 optics were used. Spectral resolution was 2 cm<sup>-1</sup>.

All water adsorption experiments were made in ultrahigh vacuum (UHV), using a system which has been described in detail previously.<sup>21</sup> The sample temperature was variable between 82 and 650 K. Reported sample temperatures are ac-

curate to within  $\pm 2^\circ$ . Dosing of D<sub>2</sub>O was performed at a base pressure of  $< 2 \times 10^{-9}$  Torr through a capillary tube ending in front of the sample, enabling repeatable doses to within  $\pm 10\%$ . The actual amount of D<sub>2</sub>O on the substrate was determined from IRAS spectra, as will be described below. IRAS measurements in the UHV system were made at a base pressure of  $< 2 \times 10^{-10}$  Torr, using 82° incidence angle, *p*-polarized light, *f*/16 optics and 2 cm<sup>-1</sup> resolution. If not stated otherwise, the UHV-IRAS spectra in this study were collected by the following procedure: (1) cooldown of the sample to the measurement temperature, (2) reference measurement, (3) D<sub>2</sub>O deposition, (4) sample measurement. The sample and reference spectra are ratioed, yielding a spectrum where only *changes* in IR absorption are visible. That is, in these “difference” spectra we only expect to see the peaks due to D<sub>2</sub>O vibrations and the peaks corresponding to frequency and/or intensity changes of the molecular vibrations of the SAM serving as substrate.

## Spectral simulation

In order to rigorously interpret spectra in a quantitative way, it is necessary to construct a physical model of the interaction of the light with the sample. One approach that has proved useful in this regard involves application of classical electromagnetic theory of wave propagation applied to a sample, whose structure is described by a parallel stack of layered media, such that each layer is optically homogeneous. This approach allows generation of explicit simulations of spectra which can be compared with the observed spectra. The detailed description of the method has been presented elsewhere,<sup>29–32</sup> and only relevant details will be presented here.

The samples are modeled as three layered structures consisting of the following: (1) D<sub>2</sub>O film layer, (2) thiolate film layer, and (3) gold substrate layer considered to be optically infinitely thick. Optical constants for gold in the desired wavelength region (2000–2780 cm<sup>-1</sup>) were obtained from the literature,<sup>33</sup> and spline fitted to generate tables of optical constants as a function of wavelength at 2 cm<sup>-1</sup> resolution. The optical properties of the thiolate layer were assumed to be wavelength independent with a value equal to the background refractive index ( $n_\infty = 1.50$ ,  $k = 0$ ) for a high density phase of polymethylene chains<sup>27</sup> due to absence of any intrinsic resonance absorption in the region (2000–2780 cm<sup>-1</sup>). A mean value of 20 Å was used for the average film thickness of all thiolate films. Minor errors in the thiolate optical constants and the thiolate layer thickness were found to have vanishingly small effects on the simulations presented below.

In the case of D<sub>2</sub>O, two reference states are available. Previous studies<sup>34,35</sup> have identified two distinctly different sets of optical constants in the relevant spectral region, one ascribed to amorphous ice (ice Ia) and the other to polycrystalline ice (ice Ih). The spectral signatures for the two forms are widely different and easily distinguished. The optical constants for these two polymorphs are available in the literature and were obtained from Bergren *et al.*<sup>34</sup> It was assumed that the molecular oscillators in the adsorbed films are

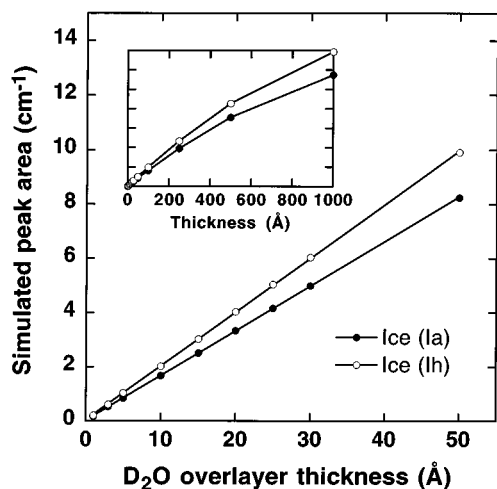


FIG. 1. Integrated intensities of simulated reflection-absorption spectra of amorphous (Ia) and polycrystalline (Ih) D<sub>2</sub>O ice, vs the overlayer thickness used in the simulation. The data shown here was used to calculate the D<sub>2</sub>O overlayer thickness for all measurements in this paper. The simulations were made using a reflection geometry with 82° incidence angle and assuming an isotropic ice overlayer on top of a 20 Å SAM on gold. See text for details.

randomly oriented and thus that the films are optically isotropic.

Next, we note that for thin films (<500 Å), the simulated spectral shape is practically independent of film thickness. Further, the integrated spectral intensity scales linearly with film thickness below 50 Å, as illustrated in Fig. 1, where integrated intensities film thickness are shown for simulated spectra of ice Ia and Ih under the experimental conditions used in our measurements. As a consequence, a simple scaling procedure can be used to obtain the best simulated spectral fit to a measured spectrum.

Finally, it should be noted that since the measured IRAS spectra are averaged over several mm<sup>2</sup> due to the size of the IR beam, the film thicknesses given are average values, revealing little or no information about the D<sub>2</sub>O film topography.

## RESULTS

### Assessment of substrate quality

It is well known that alkanethiols must exceed a certain critical hydrocarbon chain length in order to form well-ordered, all *trans*, dense SAMs. Generally, chain lengths in the range of 11–14 carbons or more are considered necessary.<sup>36,37</sup> Thus, our chosen hydrocarbon chain length of 16 carbon atoms is well in the region where formation of high-quality SAMs under appropriate conditions is expected. In the mixed monolayers, the use of TCH<sub>3</sub> and TOH allows us to maintain a virtually flat surface topography, since these molecules differ in their fully-extended length by only 1.1 Å. We thus have an ideal system for fabricating SAMs with variable wettability, while always maintaining consistent structural ordering, packing, and surface topography. Characterization of the SAMs by ellipsometry reveals that the monolayer thicknesses increase monotonically from 19 ± 1 Å

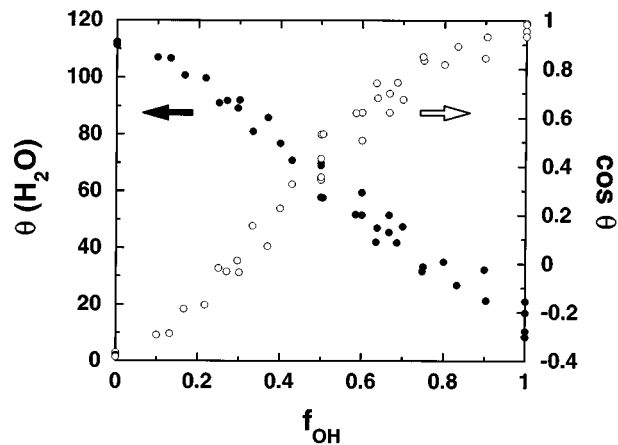


FIG. 2. Static contact angles with H<sub>2</sub>O on mixed TCH<sub>3</sub>/TOH self-assembled monolayers on gold.  $f_{OH}$  denotes the molar fraction of TOH in the preparation solution.

on  $f_{OH}=0.0$  SAMs to  $21 \pm 1$  Å on  $f_{OH}=1.0$  SAMs, where  $f_{OH}$  denotes the molar fraction of OH-terminated thiols in the self-assembly solution. IRAS measurements yield spectra with the CH<sub>2</sub>  $\nu_{as}$  [ $d^{-1}$ ] peak at 2918–2919 cm<sup>-1</sup>, which is typical for well-ordered and dense all *trans* SAMs.<sup>29,30,36</sup> Characterization of TCH<sub>3</sub>/TOH and similar mixed monolayers has also been performed earlier by us and other investigators, using IRAS,<sup>38–40</sup> XPS,<sup>20,38–43</sup> ellipsometry,<sup>39–41</sup> and contact angle measurements.<sup>20,39–44</sup>

The intentionally varied feature of the SAMs used in this investigation is the wettability. This is shown in Fig. 2 as a function of  $f_{OH}$ . The figure clearly shows how SAM samples of precisely controlled wettabilities were obtained by simply changing the solution composition of the self-assembling molecules as described in the experimental section. Since wettability is a macroscopic feature, no attempt was made to measure the extent of phase separation or precise surface distribution of the component molecules in the mixed SAMs. We refer to the well-established fact that mixed SAMs of this type show no *macroscopic* phase separation.<sup>38,40,42</sup> The fractional surface coverage of OH groups was not directly measured, but is known from previous x-ray photoelectron spectroscopy studies<sup>38,39</sup> to be close to the  $f_{OH}$  values for the TCH<sub>3</sub>/TOH system.

### D<sub>2</sub>O on substrates of varying wettability at 120 K

Figure 3 shows the IRAS spectra of D<sub>2</sub>O on SAMs of different wettability, deposited and measured at 120 K. Identical dose, yielding about three monolayers of water ( $\approx 11$  Å) on an OH-terminated surface (see below), was used for all measurements. The most intense feature in these spectra is the broad hydrogen-bonded OD stretching peak between 2200 and 2700 cm<sup>-1</sup>. There is also a weak peak at 2729 cm<sup>-1</sup>, accompanied on the most hydrophobic surfaces by a barely discernible, yet distinct peak at 2704 cm<sup>-1</sup>. Both peaks are assigned to free OD stretching vibrations.<sup>45–48</sup> Returning to the dominant absorption feature, we note that this peak is obviously composed of several overlapping compo-

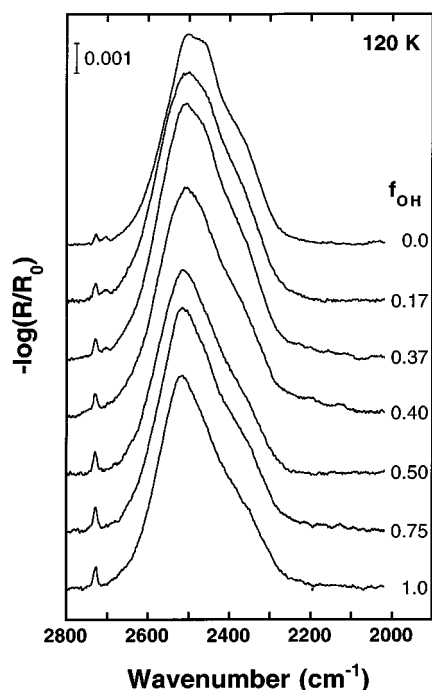


FIG. 3. IRAS spectra of D<sub>2</sub>O deposited at 120 K onto mixed SAM substrates with different composition, determined by  $f_{\text{OH}}$ . The adsorbed amount of D<sub>2</sub>O varies between approximately 2 and 3 monolayers.

nents with different relative intensities. These components originate from the  $\nu_1$  and  $\nu_3$  vibrations of the free water molecule,<sup>49</sup> but their size and shape in ice are dominated by intermolecular coupling.<sup>23,49,50</sup> Recent computer simulations and isotopic dilution experiments<sup>51</sup> indicate that modes of locally symmetric and locally antisymmetric character appear preferentially at the low- and high-frequency edges of the band, respectively.

An inspection of the figure reveals nearly constant line shape in the spectra from  $f_{\text{OH}}=1.0$  to 0.4, indicating similar structure of the D<sub>2</sub>O film on all substrates. From  $f_{\text{OH}}=0.4$  ( $\theta \sim 80^\circ$ ) and continuing to  $f_{\text{OH}}=0.0$ , there is a distinct, noticeable change in the line shape, suggesting that the D<sub>2</sub>O film adopts a different structure when deposited on the high hydrophobicity SAMs the change being largest for the most hydrophobic ( $f_{\text{OH}}=0.0$ ) SAM substrate. While deferring the detailed interpretation until the discussion section, we immediately note that the line shape of the  $f_{\text{OH}}=1.0$  to 0.4 spectra is quite comparable to that of simulated amorphous ice spectra [cf. Fig. 7(a)], while the  $f_{\text{OH}}=0.4$  to 0.0 spectra show some features qualitatively, that bear unmistakable resemblance to the simulated polycrystalline ice spectra [cf. Fig. 7(b)]. The observed peak intensity variations between substrates can be understood in terms of an interplay due to two simple effects. First, the sticking coefficient of water is lower on hydrophobic than on hydrophilic substrates at 120 K,<sup>21</sup> resulting in varying amounts of D<sub>2</sub>O being deposited on our substrates. Second, different ice polymorphs are known to have different absorption coefficients for IR radiation, which, given the structural differences implied by Fig. 3 (see above), also will influence the peak intensity.

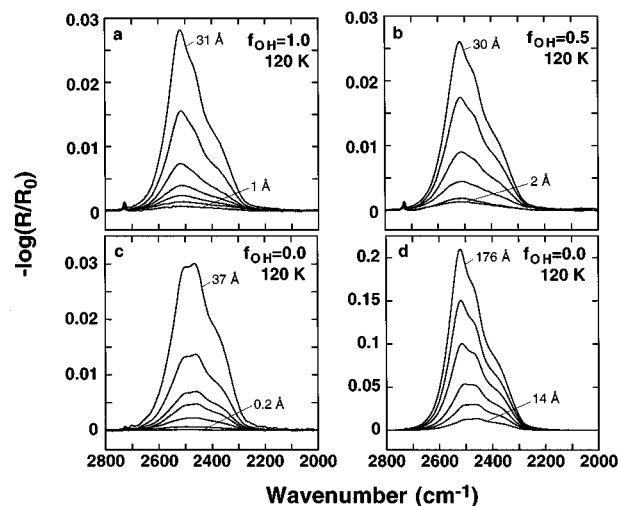


FIG. 4. IRAS spectra of varying amounts of D<sub>2</sub>O deposited at 120 K onto SAM substrates, using (a) a pure OH-terminated substrate, (b) a 1:1 mixed substrate and (c), (d) a pure CH<sub>3</sub>-terminated substrate. Note that different scales are used in (c) and (d) to highlight the progression of the peak shape as the D<sub>2</sub>O dose increases. The average thickness of the smallest and largest D<sub>2</sub>O overlayer is shown for each plot. Note that in (c) and (d), this thickness is only an approximation, since it is calculated assuming ice Ia structure of the overlayer (see text).

### Varying the dose at 120 K

Measurements for varying D<sub>2</sub>O doses were carried out on three selected substrates; the pure OH-terminated, the pure CH<sub>3</sub>-terminated, and the 1:1 mixture, with the results shown in Fig. 4. One immediately recognizes that the shapes of the OH and 1:1 spectra are very similar, whereas the CH<sub>3</sub> spectra are significantly different. This observation is consistent with the data presented in Fig. 3.

The spectra of D<sub>2</sub>O on the OH and 1:1 substrates are also similar in that the frequency of maximum absorption varies between 2513 and 2519 cm<sup>-1</sup> with the exception of the lowest coverages, where the variation is larger due to the signal to noise limitation. For D<sub>2</sub>O on the CH<sub>3</sub> substrate [Fig. 4(c)], on the other hand, this frequency varies between 2457 and 2464 cm<sup>-1</sup>, again indicating structural differences with respect to the more hydrophilic substrates. This difference in peak position persists down to peak intensities as low as  $\sim 2 \times 10^{-3}$  absorbance units (corresponding to an overlayer thickness of about 2 Å). Below this value the D<sub>2</sub>O peak still can be seen, but is largely featureless with significantly diminished resolution in the spectral features.

If we scale all the spectra in Fig. 4(a) to the same height, as is done in Fig. 5(a), differences in the spectral shape as a function of overlayer thickness become clearly evident. The increasing relative intensity of the free OD vibration (2729 cm<sup>-1</sup>) with decreasing overlayer thickness reflects the surface-to-bulk molecular ratio of the D<sub>2</sub>O overlayer and has been further analyzed in a recent paper.<sup>48</sup> Apart from this, we also see an increasing linewidth in the main OD stretching peak as we go towards low-thickness (below  $\sim 9$  Å) overlayers. The full peak width at half-maximum increases by a factor of 1.5, from 156 cm<sup>-1</sup> for the 31 Å overlayer to around 235 cm<sup>-1</sup> for the 1 Å overlayer, as shown in Fig.

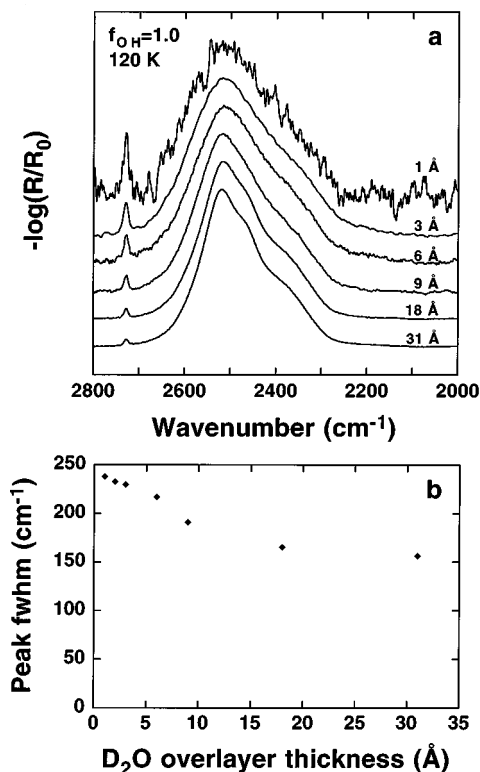


FIG. 5. (a) Spectra from Fig. 4(a), scaled to the same height to allow comparison of peak shapes and linewidths. The average thickness of the D<sub>2</sub>O ice overlayer is given for each spectrum. The apparently high noise level of the 1 Å spectrum is partly due to the scaling, and partly to the fact that the 3 Å spectrum was recorded by coaddition of 2000 interferometer scans instead of the usual 500, which decreases the noise level and makes the 1 Å spectrum appear more noisy. In (b), the full peak widths at half-maximum (FWHM) of the spectra are shown.

5(b). A significantly smaller variation is seen when the same type of scaling procedure is applied to the spectra in Fig. 4(c). In this case, the free OD vibration intensity and the main peak width both remain approximately the same for different overlayer thicknesses (not shown). The peak broadening compared to the strongest peaks is less than 15% for all but the loest coverages (below  $\sim 2$  Å), where it approaches 30%.

A further point worthy of notice is that if the D<sub>2</sub>O overlayer thickness on the CH<sub>3</sub> substrate is increased above  $\sim 100$  Å, the IRAS spectrum evolves to a shape similar to the spectrum of D<sub>2</sub>O on the OH substrate, as is evident from Fig. 4(d). The change is continuous, and at an average overlayer thickness of 150–200 Å, the spectra of D<sub>2</sub>O ice on CH<sub>3</sub> and OH substrates are virtually indistinguishable. Thus, as the overlayer is grown thicker, the polycrystalline nature of the early ice monolayers in close vicinity of the CH<sub>3</sub> substrate gradually diminishes in favor of amorphous ice structure for subsequent layers. The exact depth of persistence of the substrate-induced polycrystallinity in D<sub>2</sub>O ice layers could not be assessed, because of the gradual nature of the change.

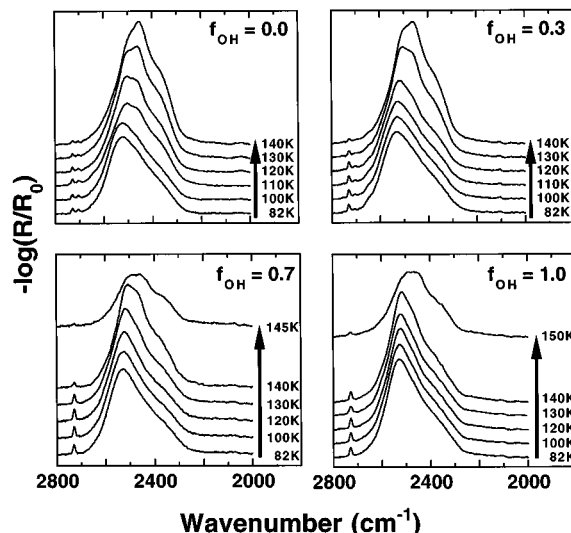


FIG. 6. Annealing of D<sub>2</sub>O on mixed SAM substrates. The deposition temperature was 82 K and consecutive IRAS spectra were taken at increasing temperatures up to 150 K. A selection of spectra at relevant temperatures is shown for each sample. See text for details.

### Annealing

In order to examine systematically the temperature dependence of the structure of adsorbed D<sub>2</sub>O, annealing experiments were made using substrates of selected different wettabilities. The substrates were dosed at 82 K, which was the lowest attainable sample temperature in our UHV configuration, and then heated to 100, 110, 120, 130, and 140 K, holding at each temperature for 5 min before measurement. A holding time of 5 min has in a previous publication<sup>21</sup> been shown to be more than sufficient for temperature-driven structural transitions in the present system to be completed. Between 140 and 150 K, the water desorbed for all substrates. On the most hydrophilic substrates, the rate of desorption was still relatively low at 145–150 K, making it possible to record an additional spectrum in this temperature interval. Representative measurements are shown in Fig. 6. At 82 K there are only minor differences between the IRAS spectra on different substrates. At higher temperatures however, the spectra undergo significant changes, the onset and evolution of which are highly dependent on substrate wettability. For the most hydrophobic substrate ( $f_{\text{OH}}=0.0$ ), the IRAS spectrum begins to alter somewhere between 100 and 110 K, whereas on the  $f_{\text{OH}}=0.3$  substrate no changes are seen until between 120 and 130 K and on the hydrophilic ( $f_{\text{OH}}=1.0$ ) substrate the spectrum remains virtually unchanged up to around the desorption temperature,  $\sim 140$  K. In control experiments, when at any point during the annealing sequence the temperature was lowered back to 82 K, the spectra remained unchanged and did not again assume their initial 82 K shape.

### DISCUSSION

At the temperatures and pressures used in these experiments, there are three possible solid forms of water;<sup>24</sup> amor-

phous ice (ice Ia), cubic ice (ice Ic), and hexagonal ice (ice Ih). The amorphous form can be further subdivided into high- and low-density forms,<sup>52</sup> and a third, “restrained” amorphous form has also been suggested.<sup>53</sup> When discussing the results in this paper, we will in turn consider amorphous ice, polycrystalline ice, and intermediate forms. High-density ice Ia exists only at temperatures below 77 K, so the amorphous ice in this study must be of the low-density or the restrained form.<sup>52,53</sup> The two crystalline forms, ice Ih and Ic, cannot be distinguished using IR data,<sup>54</sup> so we will refer to these forms only as “polycrystalline ice,” although our preparation conditions suggest that ice Ic rather than ice Ih is formed on our substrates.<sup>23,24,53</sup>

Although we cannot claim that our experiments have been conducted at thermal equilibrium, any spontaneous structural transformation from amorphous to polycrystalline ice is very slow in the temperature range used.<sup>53,55–58</sup> Previous studies<sup>57</sup> have reported measurements showing that only a mere 2%–3% of an amorphous H<sub>2</sub>O film will crystallize at 140 K during our measurement period (<10 min). The crystallization rate for D<sub>2</sub>O is known to be even lower.<sup>58</sup> The observed transitions therefore will be regarded as entirely temperature-driven phenomena, which is further supported by the combined TPD and IRAS measurements in our previous study.<sup>21</sup>

### Amorphous ice

Figure 7(a) shows a comparison between the experimental spectrum and the simulated best-fit amorphous ice spectrum for a  $f_{\text{OH}}=1.0$  substrate at 140 K. Except for a relatively minor mismatch in the line shape on the high frequency side of the spectrum, the simulated spectrum is in excellent agreement with the experimental one. This correspondence strongly proves that the spectral features of the D<sub>2</sub>O film are very well described in terms of the optical constants of amorphous solid D<sub>2</sub>O. We regard this to be extremely positive evidence suggesting amorphous structure of the adsorbed D<sub>2</sub>O film and of other D<sub>2</sub>O overlayers in this study which give rise to comparable IRAS spectra.

The excellent agreement between simulated and measured spectra in Fig. 7(a) enables us to determine the D<sub>2</sub>O overlayer thickness with high accuracy, using integrated intensities and the calibration curves presented in Fig. 1. For example, the calculated film thickness for which the best-fit spectrum in Fig. 7(a) was obtained is 13.9 Å. Thus, under the experimental conditions at hand, IRAS is demonstrated to be a useful method for thickness estimation. Further, the IRAS data can be employed to calibrate dosing procedures. We stress however that for the evaluation to be accurate, the angle of incidence must be controlled and accurately measured. A change from, e.g., 82° to 83° will result in an overall intensity increase of the simulated spectrum by a factor of 1.12.

Next, we bring to attention the fact that at sufficiently low temperatures, the spectral shapes appear nearly independent of macroscopic sample wettabilities and correlate well with simulated amorphous ice spectra [Fig. 7(a)]. These observations allow us to conclude that predominantly low-

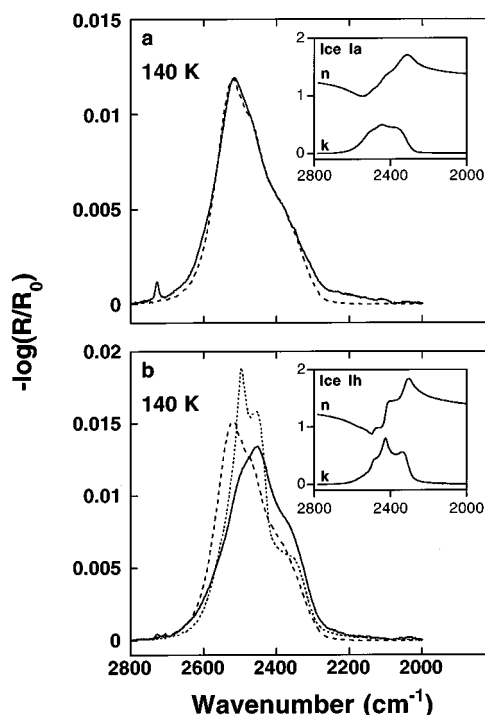


FIG. 7. IRAS spectra (solid lines) of (a) D<sub>2</sub>O on an OH-terminated substrate at 140 K, (b) D<sub>2</sub>O on a CH<sub>3</sub>-terminated substrate at 140 K, compared with simulated spectra of equal integrated area of amorphous and polycrystalline D<sub>2</sub>O ice. In (a), comparison is made only to amorphous ice (broken line), whereas in (b) comparison is made both to amorphous (broken line) and polycrystalline ice (dotted line). The insets show the optical constants (Ref. 34) of (a) ice Ia and (b) ice Ih, that were used in the simulations.

density amorphous ice is formed on all substrates at low (~82 K) temperatures. Minor yet distinct differences however are observed upon a careful comparison. These are exemplified in Fig. 8, where spectra of ice Ia at 82 K on (a) a  $f_{\text{OH}}=1.0$  and (b) a  $f_{\text{OH}}=0.0$  surface have been scaled to a common height to allow direct visual comparison. It is evident that spectrum 8b is somewhat more intense in the 2300–2500 cm<sup>-1</sup> region. A comparison with the simulated ice Ia spectrum does not yield any clues to the reasons for this discrepancy, since the simulated spectrum is not significantly closer to either of the two measured spectra. However, the subdivision of the OD stretching region into surface modes (above 2500 cm<sup>-1</sup>) and bulk modes (below 2500 cm<sup>-1</sup>) as suggested by Rowland *et al.*,<sup>47</sup> implies that the ratio of bulk to surface D<sub>2</sub>O molecules is higher on the  $f_{\text{OH}}=0.0$  surface. Since the average ice overlayer thickness is equal in the two cases, this inference directly indicates a change in ice cluster shape, favoring clusters of three-dimensional, dropletlike shape on the hydrophobic ( $f_{\text{OH}}=0.0$ ) SAMs and flatter, two-dimensional clusters on hydrophilic ( $f_{\text{OH}}=1.0$ ) SAMs. This conclusion is in direct agreement with that made from TPD data in an earlier investigation,<sup>21</sup> and is further in agreement with previous molecular dynamics simulations<sup>59</sup> and previous IR investigation of H<sub>2</sub>O films on methyl terminated thiol monolayers.<sup>60</sup>

The experimental spectra of ice Ia become increasingly similar to the simulated ones as coverage increases. For the

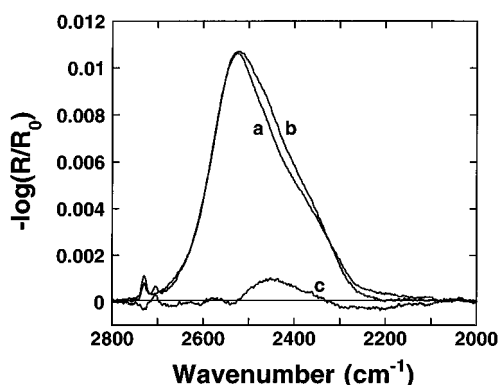


FIG. 8. IRAS spectra of amorphous D<sub>2</sub>O ice at 82 K on (a) an OH-terminated substrate and (b) a CH<sub>3</sub>-terminated substrate. The spectra were scaled to the same size to allow a direct comparison. Curve (c) is the difference between spectra a and b.

two largest peaks in Fig. 4(a) (18 and 31 Å D<sub>2</sub>O), all main features are strikingly well reproduced by the simulated spectrum. The residual error is estimated by subtracting the simulated spectrum from the measured one and comparing the area of the residual with that of the original spectrum. From the plot of residual error vs overlayer thickness in Fig. 9(a), we see that above 15–20 Å of ice, the error is consistently at ~4% in contrast to the rapidly increasing values obtained for thinner ice layers. Assuming an ice monolayer thickness of 3.66 Å,<sup>24</sup> we conclude that at coverages above ~5 monolayers, D<sub>2</sub>O ice Ia formed on hydrophilic substrates at low temperature is spectroscopically indistinguishable from bulk amorphous ice. The spectra for the thinner films, on the other hand, tend to be slightly different (larger linewidths). We believe the most plausible reason for this to be the highly delocalized nature of the vibrations of hydrogen bonded water molecules in ice.<sup>51</sup> When the D<sub>2</sub>O film thickness is smaller than an equivalent of ~5 monolayers, we can expect an increased localization of the vibrational excitations, since the long-range coupling in the direction of the surface normal would require several monolayers of D<sub>2</sub>O to be comparable to that in bulk ice. Such an increased localization would lead to a broadening of the spectral lines,<sup>51</sup> a prediction consistent with the observed spectra in Fig. 5. Of course, some accuracy is lost in the thickness estimation for the thinnest overlayers due to this broadening.

### Polycrystalline ice

In Fig. 7(b), a comparison of the best-fit simulated spectrum for each of the two available reference states (ice Ih and Ia) and the experimental spectrum for a  $f_{\text{OH}}=0.0$  substrate at 140 K is shown. It is clear that the disparities between the experimental and the calculated spectra are very large, confirming that neither amorphous nor polycrystalline ice optical constants accurately describe the observed spectral pattern, which in turn implies that the structure of the D<sub>2</sub>O layers formed on a CH<sub>3</sub> lattice is different from both bulk forms. One hint, however, is inescapable, namely that the spectral envelope in the measured spectra spans nearly the same fre-

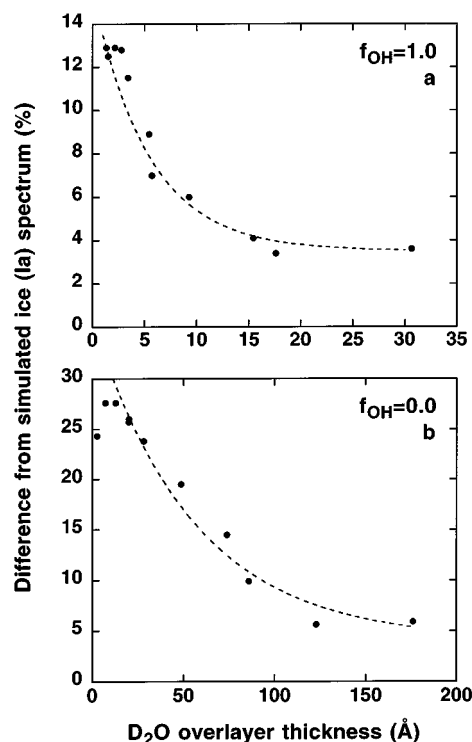


FIG. 9. Difference between simulated ice Ia spectra and measured spectra of D<sub>2</sub>O ice on (a) and OH-terminated substrate and (b) a CH<sub>3</sub>-terminated substrate at 120 K, plotted vs overlayer thickness. The difference was evaluated by (1) subtracting a simulated spectrum, scaled to minimize the residual after subtraction, from the measured spectrum; (2) integrating the residual; (3) ratioing the residual area against the area of the initial measured spectrum. Dosing and measurement were performed at 120 K. The lines are only intended as guides to the eye.

quency range as predicted by the polycrystalline model. We believe therefore that the film structure is in some perturbed state of the polycrystalline reference state. More detailed analysis of the nature of the perturbation in terms of possible factors such as orientation and inter- and intramolecular interactions is clearly desirable. Such analyses, however, are prohibitively difficult since the exact assignment of different component modes, their description in terms of free molecular vibrational modes, and assignment of correct force constants and directions of transition dipole moments in the mid-infrared frequency range, are known to be impossible.<sup>50</sup> As a result, we are forced to resort to a less quantitative, semi-empirical analysis of data.

The simulated spectral pattern due to the polycrystalline model clearly shows three distinct shoulders or peak-maxima. Similar shoulders, although significantly less pronounced, at identical peak positions are observed in the experimental spectrum. We argue that these similarities point to the possibility of representing the experimental sample with a polycrystalline model. In order to add some credence to this argument, we have subtracted the two simulated spectra in Fig. 7(b) from the experimental one, using a least-squares algorithm to choose subtraction factors that minimize the residual. By this method, the experimental spectrum is best represented by a mix of 18% of the ice Ia spectrum

and 68% of the ice Ih spectrum, plus a nonzero residual. Application of the same method to the spectra in Fig. 4(c) (D<sub>2</sub>O ice on  $f_{\text{OH}}=0.0$  substrates at 120 K) indicates that the polycrystalline nature of the film can be identified for coverages down to  $\sim 2.5$  Å (2/3 monolayer) using IRAS spectra. Films thinner than 2.5 Å yield IRAS spectra that are more similar to the simulated ice Ia spectrum than to the ice Ih spectrum. The above conclusion confirms a previous prediction by Nuzzo and co-workers<sup>35</sup> where it was proposed that a critical thickness of the ice overlayer on the order of 3 Å is required to induce temperature-driven crystallization on hydrophobic templates.

The mismatch between measured and simulated spectra could be due to contribution from several factors. For example, anisotropy of the deposited film (caused by preferential interaction with the SAM substrate), could lead to the reduction in peak-heights of vibrational components whose transition dipole moments have a major component in the plane of the metal surface, due to the surface selection rule. Another possibility is changes in the relative strengths of the contributing oscillators, caused by structural perturbations or lack of long-range order, both of which may be due to interaction with the substrate and to the low thickness of the deposited films. Last, the experimental spectrum may be representative of a mixed Ia/Ic species rather than of pure polycrystalline ice. Combinations of these effects are of course highly probable.

Another interesting observation in this regard is that when the film thickness is increased above  $\sim 100$  Å [cf. Fig. 4(d)], the spectrum of D<sub>2</sub>O ice on  $f_{\text{OH}}=0.0$  substrates at 120 K changes to a shape very close to the amorphous ice spectra in Fig. 4(a). The semblance to amorphous ice can be estimated in the same way as for ice Ia on  $f_{\text{OH}}=1.0$  substrates, by subtracting a simulated amorphous ice spectrum and evaluating the area of the remainder. A plot of the result is shown in Fig. 9(b). Note that the decreasing difference values seen for the lowest coverages are real, signifying the loss of polycrystalline ordering for thin films [cf. the lowest coverages in Fig. 4(c)]. From the plot, we estimate the influence of the SAM substrate upon the ice overlayer structure to end when an average overlayer thickness of 150–200 Å (roughly 40–55 monolayers of ice) has been reached. The exact depth of persistence of the substrate-induced polycrystallinity in D<sub>2</sub>O ice layers cannot be assessed for two reasons. First, the change is gradual, not abrupt. Second, cluster formation is expected on  $f_{\text{OH}}=0.0$  substrates.<sup>21,59</sup> The latter would leave parts of the SAM substrate bare, providing two kinds of sites for further ice adsorption; (1) on top of clusters, where amorphous ice structure is expected; (2) on the still bare parts of the SAM, where polycrystallinelike ice structure is expected. This situation may persist up to equivalent ice thicknesses of several monolayers, depending on cluster size and shape, and clearly is an obstacle to the evaluation of the depth of the surface-induced polycrystallinity. We may conclude, however, that there is an *upper* limit at  $\sim 50$  ice monolayers for the influence of the SAM substrate upon the ice structure. This is about 10 times the limit of  $\sim 5$  monolayers that was found above for ice Ia on  $f_{\text{OH}}=1.0$  substrates, which may

seem surprising, given the strong hydrogen-bonding interaction expected between the ice and the OH groups of the  $f_{\text{OH}}=1.0$  substrate. However, molecular dynamics simulations of water near highly hydrophilic and highly hydrophobic walls have been presented that also indicate much more extensive changes near the hydrophobic walls,<sup>61</sup> and thus support our results. The data presented in Fig. 9 allow us to infer the existence of an interfacial layer which is dependent on the substrate and spans the innermost monolayers of ice, with structural properties that differ from those of bulk ice.

Thickness estimation from the spectra of polycrystalline ice is more difficult than in the amorphous case, because of the larger discrepancy between simulated and measured spectra. As an example, the amorphous D<sub>2</sub>O overlayer on the  $f_{\text{OH}}=0.0$  substrate at 82 K in Fig. 6 has an average thickness of 10.6 Å by the method of peak integration. If we use simulated ice Ih spectra to calculate the thickness of the *same* overlayer at 140 K, the result is 13.6 Å. The background pressure of D<sub>2</sub>O in the UHV system is negligible, so the result is not due to further adsorption of D<sub>2</sub>O onto the sample, but must be attributed to the misfit mentioned above. Hence, absolute thickness estimations from the spectra of polycrystalline ice using the IR simulations above are to be treated with caution until after calibrations using an independent technique are made. Overlayer thicknesses given in this paper have therefore, whenever possible, been evaluated from low temperature spectra of ice Ia.

### Intermediate forms

When amorphous ice is annealed, our IRAS measurements suggest a smooth, continuous transition towards polycrystalline ice, with the D<sub>2</sub>O film taking on a number of intermediate forms in the transition temperature interval, which apparently may be of considerable width (110–140 K, cf. Fig. 6). As mentioned above, this transition region does not signify a situation of thermodynamic equilibrium; however, as discussed earlier any spontaneous annealing that occurs at constant temperature is too slow to be detectable in our experiments, and we therefore find it meaningful to refer to the intermediate forms as metastable. Other investigators have observed that upon heating ice Ia, it coexists metastably with ice Ic in certain temperature intervals,<sup>53,55</sup> which leads us to believe that our intermediates are of similar origin. This is also an indication that the polycrystalline ice formed in our experiments is ice Ic rather than Ih. The maximum observed percentages of ice Ia converted to Ic in the cited papers were 30% (Ref. 55) and around 50%,<sup>53</sup> respectively.

The assumption of mixed Ia/Ic ice provides no immediate explanation of the observed IRAS spectra, though. It is impossible to generate matches to our intermediate spectra by linear combination of the simulated ice Ia and Ih spectra or optical constants, or by combination of one amorphous-like and one polycrystallinelike experimental spectrum, such as those in Figs. 7(a) and 7(b). Hence, we are unable to quantify the relative amount of ice Ia in the intermediate films, or even to confirm whether the intermediates are mixtures of amorphous and polycrystalline ice, or “true” inter-

mediate forms, which are neither amorphous nor polycrystalline.

As can be seen from Fig. 6, the molecular composition of the SAM substrate has a large influence on the transition onset temperature and on the extent to which polycrystalline ice is formed before the overlayer desorbs. The direct cause of this is the hydrogen bonds that form between D<sub>2</sub>O molecules and the surface hydroxyls of the SAM. The hydrogen bonds cannot be verified directly from IRAS spectra, but strong evidence of their existence in a similar system [D<sub>2</sub>O on Au-S(CH<sub>2</sub>)<sub>15</sub>COOCH<sub>3</sub> SAMs] has been put forward in a recent paper by us.<sup>22</sup> As a result of the hydrogen bond formation, the ice overlayer will be pinned to the SAM substrate, more strongly for SAMs with large  $f_{\text{OH}}$  (hydrophilic monolayers) than with small  $f_{\text{OH}}$  (hydrophobic monolayers). Since the lattice structure of the SAM is incommensurate with the ice Ic (and Ih) structure, such a pinning will impede the structural rearrangement from amorphous to polycrystalline ice. The number of hydrogen bonds that must be broken to achieve the rearrangement should, in a first approximation, be proportional to  $f_{\text{OH}}$ . The above scenario is consistent with the observed transition onset which occurs at increasing temperature for increasing  $f_{\text{OH}}$  as can be concluded from Fig. 6.

In the interpretation of the structural transition, difference spectra can be used to highlight the successive changes from the initial amorphous state. An example is shown in Fig. 10, where the spectra of D<sub>2</sub>O on a  $f_{\text{OH}}=0.6$  substrate are plotted for 82, 100, 120, 130, and 140 K, together with the difference spectra which result when the 82 K spectrum is subtracted from the four other ones obtained at higher temperatures (subtraction factor 1.000). Any interpretation of these difference spectra must be viewed very critically, since we are comparing ice overlayers having different structure. However, some aspects deserve to be mentioned. It is evident from the difference spectra that as the band shape evolves towards a polycrystallinelike ice spectrum, there is a lowering of intensity in the region above 2530 cm<sup>-1</sup> and an increase below 2530 cm<sup>-1</sup>. Adopting the assignment of the region above 2500 cm<sup>-1</sup> to surface vibrational modes of ice and the region below 2500 cm<sup>-1</sup> to bulk modes, as suggested in a recent paper,<sup>47</sup> this means a reduction of surface modes and an increase of bulk modes as the ice is annealed.

Aside from the direct interpretation, the difference spectra in Fig. 10 also provide a means of determining how far from the original amorphous state that the ice overlayer has evolved. For example, the 82 and 100 K spectra, which are practically identical, generate a difference spectrum that is almost a straight line. The integrated area of the absolute value of this difference spectrum, ratioed against the area of the amorphous 82 K spectrum, then yields a measure of the change. For the 100 K spectrum, this change is a mere 2%; for the 140 K spectrum, it is 32%. As a comparison, the difference between simulated ice Ia and Ih spectra by the same method is 34%. In view of the subdivision of overlayer structures into amorphous-transition-polycrystalline forms discussed above, it seems reasonable to define the onset of the phase transition at a certain spectral change percentage;

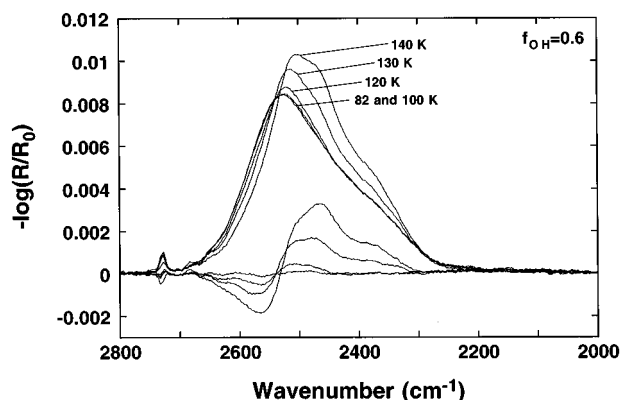


FIG. 10. An annealing experiment, identical to the ones presented in Fig. 6, showing IRAS spectra at 82, 100, 120, 130, and 140 K. Further included are four curves, showing the difference between the 100, 120, 130, and 140 K measurements and the initial 82 K measurement.

in this report, we have arbitrarily chosen a value of 10%. By linear interpolation between the actual measurements, the sample temperature at which the phase transition onset occurs may then be approximately determined and plotted vs  $f_{\text{OH}}$  in a tentative phase diagram, as shown in Fig. 11, where filled circles indicate onsets calculated with the 10% limit.

The end of the phase transition is more elusive, and difficult to pinpoint using the same approach. Indeed, since we cannot with certainty identify a 100% polycrystalline ice overlayer in any of the measurements performed, the concept of an end of the phase transition is irrelevant and unjustifiably speculative under the present experimental conditions. However, it is easily seen from the measured spectra that at any given temperature above the transition onset, the transition towards polycrystalline ice has evolved further for smaller than for larger  $f_{\text{OH}}$ . Thus, if we indicate the gradual transition towards polycrystalline ice by increasingly darker shades of gray in the phase diagram of Fig. 11, a qualitative view emerges where the highest crystallinity is found for low  $f_{\text{OH}}$  values and high temperatures.

Next, we consider the results of previous TPD measurements.<sup>21</sup> The TPD peak temperature on substrates with different  $f_{\text{OH}}$  is drawn as a thick line at the rightmost end of the phase diagram. The reader is cautioned that the peak temperature varies with initial coverage, and thus that the line in Fig. 11 only indicates *representative*, not absolute, values. To enable comparison, care has been taken to evaluate the peak temperature for identical initial coverages throughout the  $f_{\text{OH}}$  range. We have interpreted the sudden increase around  $f_{\text{OH}}=0.6$  as reflecting the limit where the phase transition, from being complete at low  $f_{\text{OH}}$ , no longer is completed prior to desorption from the substrate. Direct support of this interpretation from the present IRAS measurements is not possible to obtain though, since the rate of desorption above 150 K is too high to allow collection of IRAS spectra. IRAS measurements around  $f_{\text{OH}}=0.6$  at lower temperatures reveal no D<sub>2</sub>O film characteristics different from those on other ( $f_{\text{OH}} \neq 0.6$ ) substrates. The TPD data and their interpretation, together with the rest of the tentative

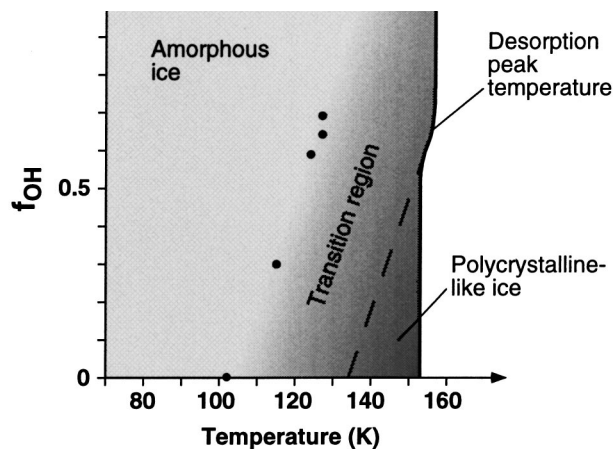


FIG. 11. Tentative phase diagram for thin D<sub>2</sub>O ice overlayers on mixed TCH<sub>3</sub>/TOH substrates. The diagram is divided into two sections—amorphous ice and a transition region where the structure gradually changes towards polycrystalline ice. The thick line in the 150–160 K region indicates the thermal desorption peak temperature for D<sub>2</sub>O from these surfaces, as it has been presented in a previous publication (Ref. 21). The onset of the transition region was arbitrarily defined as the temperature where the IRAS spectrum of the overlayer has evolved to differ with 10% from its initial shape (characteristic of amorphous ice) at 82 K, and is indicated by filled circles.

phase diagram, would mean that there is a triangular region in the lower right corner of Fig. 11, approximately defined by a line from the increase at ( $T=153$  K;  $f_{\text{OH}}=0.6$ ) to ( $T=134$  K;  $f_{\text{OH}}=0.0$ ), where the phase transition has proceeded to completion. However, since the TPD peak temperatures are not absolute, the region can not be unambiguously determined. Our IRAS data, which indicate significant progression of the transition between  $T=130$  and  $140$  K for  $f_{\text{OH}}=0.0$ , suggest a smaller window. Further, considering the above discussion of mixed Ia/Ic ice, we stress that completion of the phase transition under our experimental conditions does not necessarily mean that the D<sub>2</sub>O overlayer is 100% polycrystalline. Consequently, we prefer the label polycrystalline-like ice for this region.

## CONCLUSIONS

Simulated IRAS spectra may successfully be used to identify amorphous D<sub>2</sub>O ice on mixed SAM substrates, and to determine the average thickness of the ice overlayer. The structural transition towards polycrystalline ice as the sample is annealed can be monitored, but for the thin films investigated here, the agreement with simulated ice Ih spectra is poor, suggesting at best polycrystalline-like overlayers. A possible reason for this is interaction between the overlayer and the SAM substrate. Hydrophobic (pure CH<sub>3</sub>-terminated) SAMs are shown to structurally influence the ice overlayer up to an average coverage of  $\sim 50$  monolayers, which may be why the spectral signature of bulk polycrystalline ice, which is known to be highly dependent on long-range molecular interaction, is not reproduced for D<sub>2</sub>O on these SAMs. Hydrophilic (pure OH-terminated) SAMs also influence the ice structure, but this effect seems limited to aver-

age coverages below  $\sim 5$  monolayers. We believe that these values of 5 vs 50 monolayers reflect the importance of cluster size and shape for the ice structure.

Annealing experiments show that the onset of the structural transition is highly dependent on the composition of the SAM substrate. This seems reasonable, since the investigated ice overlayers mostly are in the range of 2–3 monolayers in thickness, and thus can be expected to be influenced in their entirety by hydrogen bonding or other interaction with the SAM. One must consequently consider the possibility that the structural progression caused by annealing of these thin films may differ from that of bulk ice. This substrate-induced effect could then account for the “intermediate” forms seen in the annealing experiments. Further experiments are needed to establish whether the substrate–overlayer interaction is prominent enough to make these intermediate forms thermodynamically stable, or if they should be considered metastable, with a large time constant governing the progression towards polycrystalline ice. The tentative phase diagram in Fig. 11, summarizing our findings for thin ice overlayers on mixed SAMs, is therefore only valid for the experimental conditions used in this investigation.

Further investigations of the D<sub>2</sub>O ice/mixed SAM system, covering aspects like ice–SAM interaction, sticking, and clustering, have recently been presented in another paper.<sup>48</sup>

## ACKNOWLEDGMENT

This work was supported by a grant from the Swedish Research Council for Engineering Sciences.

- <sup>1</sup>R. G. Nuzzo and D. L. Allara, *J. Am. Chem. Soc.* **105**, 4481 (1983).
- <sup>2</sup>Ulman, *An Introduction to Ultrathin Organic Films from Langmuir–Blodgett to Self-Assembly* (Academic, San Diego, 1991).
- <sup>3</sup>K. D. Schierbaum, T. Weiss, E. U. Thoden van Velzen, J. F. J. Engbersen, D. N. Reinhoudt, and W. Göpel, *Science* **265**, 1413 (1994).
- <sup>4</sup>L. Häussling, H. Ringsdorf, F.-J. Schmitt, and W. Knoll, *Langmuir* **7**, 1837 (1991).
- <sup>5</sup>G. P. López, M. W. Albers, S. L. Schreiber, R. Carroll, E. Peralta, and G. M. Whitesides, *J. Am. Chem. Soc.* **115**, 5877 (1993).
- <sup>6</sup>K. L. Prime and G. M. Whitesides, *Science* **252**, 1164 (1991).
- <sup>7</sup>Y. Maeda, H. Yamamoto, and H. Kitano, *J. Phys. Chem.* **99**, 4837 (1995).
- <sup>8</sup>C. D. Frisbie, L. F. Rozsnyai, A. Noy, M. S. Wrighton, and C. M. Lieber, *Science* **265**, 2071 (1994).
- <sup>9</sup>A. Noy, C. D. Frisbie, L. F. Rozsnyai, M. S. Wrighton, and C. M. Lieber, *J. Am. Chem. Soc.* **117**, 7943 (1995).
- <sup>10</sup>K. Konstadinidis, P. Zhang, R. L. Opila, and D. L. Allara, *Surf. Sci.* **338**, 300 (1995).
- <sup>11</sup>P. E. Laibinis and G. M. Whitesides, *J. Am. Chem. Soc.* **114**, 9022 (1992).
- <sup>12</sup>L. M. Frostman, M. M. Bader, and M. D. Ward, *Langmuir* **10**, 576 (1994).
- <sup>13</sup>R. A. Drawhorn and N. L. Abbott, *J. Phys. Chem.* **99**, 16 511 (1995).
- <sup>14</sup>N. Nakashima and T. Taguchi, *Colloids and Surfaces A* **103**, 159 (1995).
- <sup>15</sup>A. Kumar and G. M. Whitesides, *Science* **263**, 60 (1994).
- <sup>16</sup>A. Kumar, H. A. Biebuyck, and G. M. Whitesides, *Langmuir* **10**, 1498 (1994).
- <sup>17</sup>J. Huang, D. A. Dahlgren, and J. C. Hemminger, *Langmuir* **10**, 626 (1994).
- <sup>18</sup>M. F. Colombo, D. C. Rau, and V. A. Parsegian, *Science* **256**, 655 (1992).
- <sup>19</sup>D. Hanein, B. Geiger, and L. Addadi, *Langmuir* **9**, 1058 (1993).
- <sup>20</sup>A. Ulman, S. D. Evans, Y. Shnidman, R. Sharma, and J. E. Eilers, *Adv. Colloid Int. Sci.* **39**, 175 (1992).
- <sup>21</sup>I. Engquist, I. Lundström, and B. Liedberg, *J. Phys. Chem.* **99**, 12 257 (1995).

- <sup>22</sup>I. Engquist, M. Lestelius, and B. Liedberg, *J. Phys. Chem.* **99**, 14 198 (1995).
- <sup>23</sup>J. P. Devlin, *Int. Rev. Phys. Chem.* **9**, 29 (1990).
- <sup>24</sup>P. V. Hobbs, *Ice Physics* (Clarendon, Oxford, 1974).
- <sup>25</sup>J. P. Devlin and V. Buch, *J. Phys. Chem.* **99**, 16 534 (1995).
- <sup>26</sup>F. L. A. McCrackin, NBS Technical Note, 1969.
- <sup>27</sup>J. Shi, B. Hong, A. N. Parikh, R. W. Collins, and D. L. Allara, *Chem. Phys. Lett.* **246**, 90 (1995).
- <sup>28</sup>A. Ihs, B. Liedberg, K. Uvdal, C. Törnkvist, P. Bodö, and I. Lundström, *J. Colloid Interface Sci.* **140**, 192 (1990).
- <sup>29</sup>D. L. Allara and R. G. Nuzzo, *Langmuir* **1**, 52 (1985).
- <sup>30</sup>A. N. Parikh and D. L. Allara, *J. Chem. Phys.* **96**, 927 (1992).
- <sup>31</sup>A. Ihs, K. Uvdal, and B. Liedberg, *Langmuir* **9**, 733 (1993).
- <sup>32</sup>N.-O. Persson, K. Uvdal, B. Liedberg, and M. Hellsten, *Progress Colloid Polym. Sci.* **88**, 100 (1992).
- <sup>33</sup>E. D. Palik, *Handbook of Optical Constants of Solids* (Academic, London, 1985).
- <sup>34</sup>M. S. Bergren, D. Schuh, M. G. Sceats, and S. A. Rice, *J. Chem. Phys.* **69**, 3477 (1978).
- <sup>35</sup>R. G. Nuzzo, B. R. Zegarski, E. M. Korenic, and L. H. Dubois, *J. Phys. Chem.* **96**, 1355 (1992).
- <sup>36</sup>M. D. Porter, T. B. Bright, D. L. Allara, and C. E. D. Chidsey, *J. Am. Chem. Soc.* **109**, 3559 (1987).
- <sup>37</sup>P. Fenter, P. Eisenberger, and K. S. Liang, *Phys. Rev. Lett.* **70**, 2447 (1993).
- <sup>38</sup>L. Bertilsson and B. Liedberg, *Langmuir* **9**, 141 (1993).
- <sup>39</sup>A. N. Parikh, B. Liedberg, S. V. Atre, M. Ho, and D. L. Allara, *J. Phys. Chem.* **99**, 9996 (1995).
- <sup>40</sup>S. V. Atre, B. Liedberg, and D. L. Allara, *Langmuir* **11**, 3882 (1995).
- <sup>41</sup>J. P. Folkers, P. E. Laibinis, and G. M. Whitesides, *Langmuir* **8**, 1330 (1992).
- <sup>42</sup>C. D. Bain, J. Evall, and G. M. Whitesides, *J. Am. Chem. Soc.* **111**, 7155 (1989).
- <sup>43</sup>C. D. Bain, H. A. Biebuyck, and G. M. Whitesides, *Langmuir* **5**, 723 (1989).
- <sup>44</sup>A. Ulman, S. D. Evans, Y. Shnidman, R. Sharma, J. E. Eilers, and J. C. Chang, *J. Am. Chem. Soc.* **113**, 1499 (1991).
- <sup>45</sup>B. W. Callen, K. Griffiths, and P. R. Norton, *Surf. Sci. Lett.* **261**, L44 (1992).
- <sup>46</sup>A. B. Horn, M. A. Chesters, M. R. S. McCoustra, and J. R. Sodeau, *J. Chem. Soc. Faraday Trans.* **88**, 1077 (1992).
- <sup>47</sup>B. Rowland, N. S. Kadagathur, J. P. Devlin, V. Buch, T. Feldman, and M. J. Wojcik, *J. Chem. Phys.* **102**, 8328 (1995).
- <sup>48</sup>I. Engquist and B. Liedberg, *J. Phys. Chem.* **100**, 20089 (1996).
- <sup>49</sup>E. Whalley, *Can. J. Chem.* **55**, 3429 (1977).
- <sup>50</sup>S. A. Rice, M. S. Bergren, A. C. Belch, and G. Nielson, *J. Phys. Chem.* **87**, 4295 (1983), and references therein.
- <sup>51</sup>M. J. Wojcik, V. Buch, and J. P. Devlin, *J. Chem. Phys.* **99**, 2332 (1993).
- <sup>52</sup>A. H. Narten, C. G. Venkatesh, and S. A. Rice, *J. Chem. Phys.* **64**, 1106 (1976).
- <sup>53</sup>P. Jenniskens and D. F. Blake, *Science* **265**, 753 (1994).
- <sup>54</sup>J. E. Bertie and E. Whalley, *J. Chem. Phys.* **40**, 1637 (1964).
- <sup>55</sup>L. G. Dowell and A. P. Rinfret, *Nature* **188**, 1144 (1960).
- <sup>56</sup>*Water and Aqueous Solutions at Subzero Temperatures*, edited by F. Franks (Plenum, New York, London, 1982), Vol. 7.
- <sup>57</sup>W. Hage, A. Hallbrucker, and E. Mayer, *J. Chem. Phys.* **100**, 2743 (1994).
- <sup>58</sup>W. Hage, A. Hallbrucker, E. Mayer, and G. P. Johari, *J. Chem. Phys.* **103**, 545 (1995).
- <sup>59</sup>J. Hautman and M. L. Klein, *Phys. Rev. Lett.* **67**, 1763 (1991).
- <sup>60</sup>L. H. Dubois, B. R. Zegarski, and R. G. Nuzzo, *J. Am. Chem. Soc.* **112**, 570 (1990).
- <sup>61</sup>J. R. Grigera, S. G. Kalko, and J. Fischbarg, *Langmuir* **12**, 154 (1996).